BIBECHANA
Vol. 23, No. 2, April 2026, 129-145

ISSN 2091-0762 (Print), 2382-5340 (Online)
Journal homepage: http://nepjol.info/index.php/BIBECHANA
Publisher:Dept. of Phys., Mahendra Morang A. M. Campus (Tribhuvan University)Biratnagar

Structural, elastic, and, strain induced electronic and magnetic properties of half-Heusler alloys MnSnX (X = Ni, Cu, and Pd)

Uchit Chaudhary[1,2], Subash Dahal[1*], Bhupal Guragain[1], Gopi Chandra Kaphle[2], Shashit Kumar Yadav[1*]

[1]*Department of Physics, Mahendra Morang Adarsh Multiple Campus, Tribhuvan University Biratnagar, Nepal.*
[2]*Central Department of Physics, Tribhuvan University, Kirtipur, Nepal.*

*Corresponding authors: Email: sashit.yadav@mmamc.tu.edu.np;subashdahal15@gmail.com

Abstract

Half-metallic (HM) ferromagnetic materials have garnered significant attention due to their potential applications in solid-state electronic devices. Strain manipulation offers a promising avenue for tuning the physical properties of such materials. In this regard, the structural, elastic, and strain effect on electronic and magnetic properties of half-Heusler MnSnX (X = Ni, Cu, and Pd) alloys have been studied in this work. Our findings revealed that these compounds exhibit negative formation and cohesive energies, indicative of their chemical stability and potential for experimental synthesis, with the exception of MnSnCu. Elastic property analysis further demonstrated the mechanical stability of all compounds, yet their inherent brittleness. We observed HM behaviour under uniform compressive strain ranging from -5% to -14% in MnSnNi and MnSnPd, with band gaps between 0.499 and 0.822 eV calculated using the GGA method whereas MnSnCu remains metallic under applied strains. The mBJ method further validated HM characteristics, except for MnSnCu under compressive strains from -6% to -9% for MnSnNi and -12% to -14% for MnSnPd. The magnetic properties under uniform compressive strains, where HM nature is achieved, conform to the Slater-Pauling 18-electron rule, and exhibit 100% spin polarization at the Fermi level. This polarization primarily stems from the transition metal Mn, with minor contributions from Ni, Pd, and Sn. In light of our findings, we propose that the electronic and magnetic attributes of these materials can be enhanced through the application of strains, potentially making them attractive for spintronic applications.

Keywords
Half-metallic, electronic properties, magnetic properties, spin polarization, spintronic.

Article information
Manuscript received: January 1, 2026; Revised: March 20, 2026; Accepted: March 28, 2026
DOI https://doi.org/10.3126/bibechana.v23i2.93913

1 Introduction

Many research reports have been carried out on the possibility of half-metallicity (HM) in the half-Heusler (HH) alloys both experimentally and theoretically since 1983, when de Groot and his colleagues made a stunning finding about the half-metallic feature of NiMnSb half-Heusler alloy [1]. HH alloys have gained attention in recent years due to their unique combination of properties, particularly their HM, which makes them promising materials. HM behavior, which refers to the fact that one of the spin channel in the electronic structure exhibits metallic behavior, while the other is completely (100%) spin polarized at the Fermi level [1], [2], [3]. There are three types of Heusler compounds: full, half, and inverse [4], [5]. Each type has a unique formula: X_2YZ for full, XYZ for half, and XYXZ for inverse. X and Y in these compounds represent high and low valent transition metals, while Z denotes an atom with sp electrons. Full-Heusler (FH) compounds crystallize in $L2_1$ having four FCC sublattices [6] and HH in $C1_b$ structures through space group $F\bar{4}3m$ (No. 216) where one of the sublattice is left unoccupied [7]. Both the FH and HH follow a Slater-Pauling behavior $M_t = Z_t - 24$ and $M_t = Z_t - 18$, respectively [8], [9], where M_t is the total magnetic moment, Z_t is the total number of valence electrons. HH alloys typically exhibit lower magnetic moments and Curie temperatures than FH alloys [10], [11], [12], [13]. Djaafri et al. investigated HM behavior with total magnetic moments 1 μ_B and 3 μ_B per unit cell for ReCrTe and RuCrTe, respectively [14]. The structural, mechanical, electronic, and transport properties of HH RuVX (As, P, and Sb) compounds also have been studied [15]. Rahman et al. reported HH ScTiX (X = Si, Ge, Pb, In, As, and Tl) compounds to be HM near the Fermi level [16]. Moreover, the elastic properties showed that all the compounds are brittle in nature, except ScTiSi. Shakil et al. observed metallic character in LiCrP and LiCrAs while half-metallic character in LiCrBi and LiCrSb alloys with 100% spin polarization [17].

Bennani et al. studied compounds RhFeX (X = Ge, Sn), finding them to be HM ferromagnets following the Slater-Pauling rule with 100% spin polarization near the Fermi level [18]. Shakil et al. investigated HM nature in HH KMnZ (Z = B, Si, Ge, As) alloys in minority-spin channels. They reported minority band gaps for KMnB, KMnSi, KMnGe, and KMnAs of 0.60, 0.85, 1.00, and 1.20 eV, respectively [19]. Radouan et al. investigated half-metallic ferromagnetic (HMF) nature in both SiLiSr alloy and SiLiCa, with a direct band gap of 1.401 eV and a HM gap of 0.42 eV for SiLiSr, and an indirect gap of 0.21 eV and HM gap of 0.401 eV for SiLiCa [20]. The HM nature has been investigated in many more compounds such as CrTiX (X = Si, Ge, Sn, Pb) [21], RuMnZ (Z = P, As) [22], and CrVZ (Z = S, Se, Te) [23]. Further, Khandy et al. investigated strain effects on structural, electronic, and phonon properties of the newly proposed HH compound SrBaSn [24]. The direct band gap reduced to 0.19 eV from 0.70 eV at +12% strain, beyond which the structure becomes unstable. However, an indirect gap ranging from 0.63 eV to 0.39 eV is observed in the strain range of +5% to +8%. The suitability of materials for various technological applications depends on their electronic and magnetic properties. Metallic materials have gained widespread application across various domains due to their notable attributes such as excellent electrical conductivity and strong mechanical properties [25], [26], [27]. However, their electronic and magnetic properties may not always meet the requirements of magneto-electronics and spintronics applications [28], [29], such as spin filters [30], spin injection [31], tunnel junctions [32], [33], and giant magneto-resistance devices [34], [35]. In contrast, HM materials display distinct electronic and magnetic behavior that renders them potential candidates for these applications.

Recently, scientists have been exploring ways to modify the properties of both metallic and HM materials using strain, which refers to deformation caused by external forces applied to the material. The application of strain can alter the band structure, density of states, magnetic moment, magnetic anisotropy, and magnetic ordering of materials [36], [37], [38]. The resulting modifications can have important implications for the performance and functionality of materials in various magneto-electronics and spintronics applications.

The theoretical and experimental studies mentioned earlier have inspired us to gain deeper insight into the electronic and magnetic properties of HH alloys MnSnX (X = Ni, Cu, and Pd). Here, we explore the electronic and magnetic properties of these HH alloys using density functional theory (DFT) calculations via strain engineering within the generalized gradient approximation (GGA), generalized gradient approximation plus U (GGA+U), and modified Becke–Johnson (mBJ) methods in this work.

2 Theoretical and computation details

We have used the full-potential linearized augmented plane-wave (FP-LAPW) method [39] as implemented in the WIEN2k code [40], [41], [42], [43] to calculate the electronic and magnetic proper-

ties of HH MnSnX (X = Ni, Cu, and Pd) alloys. The GGA [44], GGA plus U (GGA+U) [45], [46], and mBJ [47], [45] have been used separately as exchange-correlation functionals. We have used $U = 2$ eV and $J = 0.0$ eV for the description of correlation effects in the localized Mn-d orbital in all calculations [48]. For the wave function expansion inside the atomic spheres, the maximum value of $L_{\max} = 10$ was chosen, and the plane-wave cutoff was set to $R_{mt} \times K_{max} = 7$ with $G_{max} = 12$. A 17×17×17 k-mesh grid with 165 k-points within the irreducible wedge of the Brillouin zone was found to be well converged. The self-consistent calculations were achieved with an energy convergence criterion of 10^{-4} Ry and charge convergence of 10^{-3} electrons. The muffin-tin radii (R_{mt}) were chosen in the range of 2.39 to 2.50 (a.u.), which vary for each atom depending on their size, and the cutoff energy was set to −6.0 Ry.

3 Results and discussion

3.1 Structural properties

It has been found that MnSnX (X = Ni, Cu, and Pd) crystallizes into a cubic structure of type MgAgAs that is compatible with the space group F$\bar{4}$3m (No. 216). The Wyckoff positions for Mn, Sn, and X are at $(1/2, 1/2, 1/2)$, $(0, 0, 0)$, and $(1/4, 1/4, 1/4)$, respectively, as shown in Figure 1(a). The magnetic ground state properties are determined by minimizing the total energy as a function of volume for both magnetic and non-magnetic (NM) states. The total energy versus volume in ferromagnetic (FM) and NM phases for all compounds are depicted in Figure 1(b–d). It is found that the FM state is more stable than the NM state due to its lower minimum total energy. Moreover, the energy difference ($\Delta E = E_{\rm FM} - E_{\rm NM}$) is negative, indicating that the FM state is energetically more favorable than the NM phase.

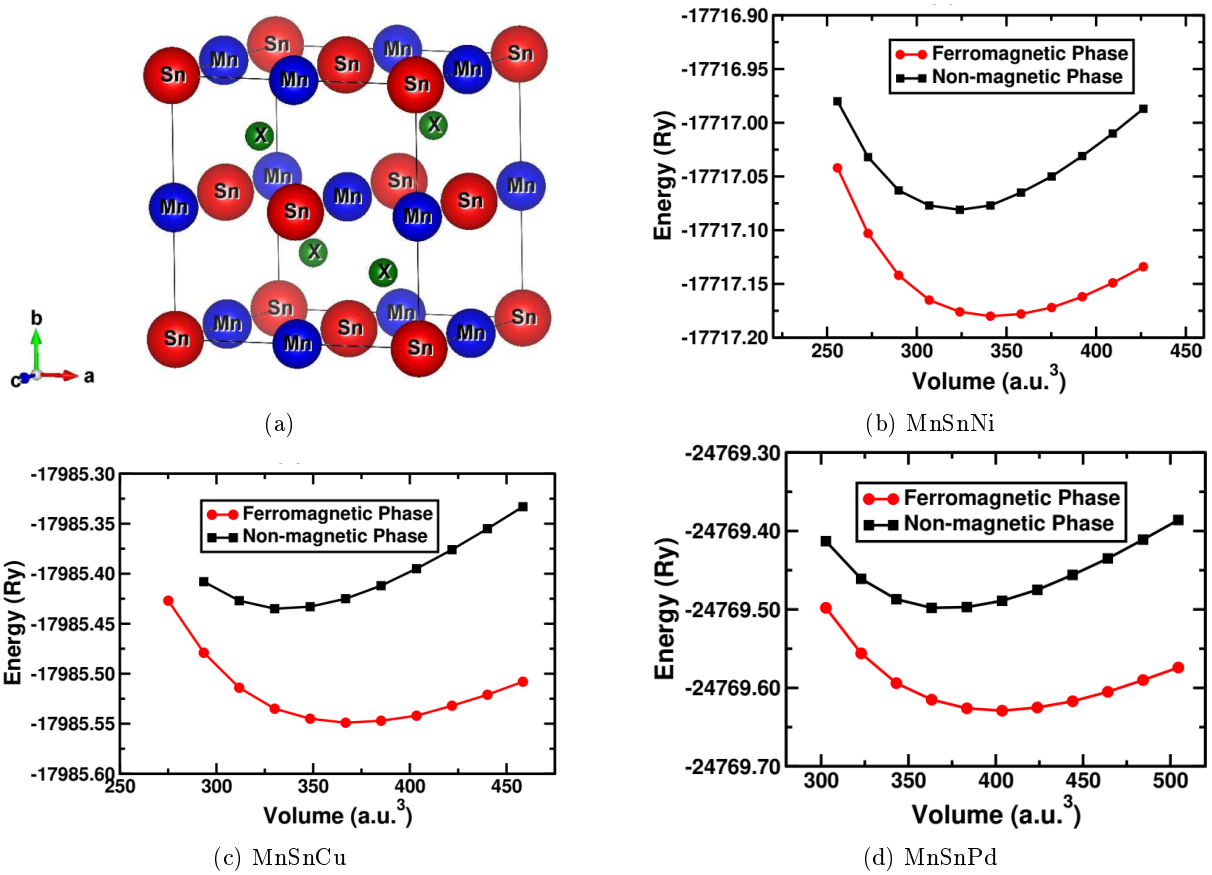

(a) (b) MnSnNi

(c) MnSnCu (d) MnSnPd

Figure 1: (a) Optimized crystal structure (b-d) structural volume optimization of half-Heusler MnSnX (X=Ni, Cu, and Pd) alloys.

Further, geometrical optimization calculations have been performed to obtain the equilibrium lattice constant by fitting the Birch–Murnaghan equation of state [49] to the total energy versus volume data for three possible phases (Type 1, Type 2, and Type 3), in order to determine the correct atomic arrangement in the crystal, as shown in Figure 1A (see Appendix).

It is noted that all the compounds are most stable in Type 1, and hence the structural, elastic, electronic, and magnetic properties are calculated for Type 1 only. The optimized results for lattice parameters (a), bulk modulus (B), and its derivative (B'), equilibrium volume (V_0) and energy (E_0), formation (E_f) and cohesive (E_c) energies, and the energy difference between FM and NM phases ($\Delta E_{\mathrm{FM-NM}}$) for all these compounds are presented in Table 1.

Table 1: The lattice parameter (a), bulk modulus (B) and its first derivative (B'), equilibrium volume (V_0) and energy (E_0), formation energy (E_f), cohesive energy (E_c), and energy difference between ferromagnetic (FM) and non-magnetic (NM) phases ($\Delta E_{\mathrm{FM-NM}}$) for half-Heusler MnSnX (X = Ni, Cu, and Pd) alloys.

Parameter	**Compound**		
	MnSnNi	MnSnCu	MnSnPd
a (Å)	5.8734	6.0241	6.1904
B (GPa)	103.8750	85.9172	94.5166
B'	5.3074	4.9199	4.9458
V_0 (a.u.^{3})	341.8179	368.8203	400.2058
E_0 (Ry)	-17717.180300	-17985.549063	-24769.628668
E_f (eV/atom)	-0.107	0.033	-0.235
E_c (eV/atom)	-3.893	-3.330	-3.695
$\Delta E_{\mathrm{FM-NM}}$ (eV)	-1.3522	-1.5534	-1.7718

Further, E_f and E_c were estimated to confirm the chemical stability of HH MnSnX (X = Ni, Cu, and Pd) alloys by using the following equations [18], [41], [42]:

$$E_f = E^{\mathrm{total}}_{\mathrm{MnSnX}} - \left(E^{\mathrm{bulk}}_{\mathrm{Mn}} + E^{\mathrm{bulk}}_{\mathrm{Sn}} + E^{\mathrm{bulk}}_{\mathrm{X}}\right) \quad (1)$$

$$E_c = E^{\mathrm{total}}_{\mathrm{MnSnX}} - \left(E^{\mathrm{iso}}_{\mathrm{Mn}} + E^{\mathrm{iso}}_{\mathrm{Sn}} + E^{\mathrm{iso}}_{\mathrm{X}}\right) \quad (2)$$

where $E^{\mathrm{total}}_{\mathrm{MnSnX}}$ is the total energy of MnSnX in a unit cell, and $E^{\mathrm{bulk}}_{\mathrm{Mn}}$, $E^{\mathrm{bulk}}_{\mathrm{Sn}}$, and $E^{\mathrm{bulk}}_{\mathrm{X}}$ are the total energies per atom at ambient temperature in their standard states. $E^{\mathrm{iso}}_{\mathrm{Mn}}$, $E^{\mathrm{iso}}_{\mathrm{Sn}}$, and $E^{\mathrm{iso}}_{\mathrm{X}}$ are the isolated atomic energies of Mn, Sn, and X, respectively.

The calculated values of E_f (E_c) are -0.107 (-3.893), 0.033 (-3.330), and -0.235 (-3.695) eV/atom for MnSnNi, MnSnCu, and MnSnPd, respectively (Table 1). Our results are in good agreement with the results extracted from the Open Quantum Materials Database (OQMD) [50], [51]. The negative values of E_f and E_c for MnSnNi and MnSnPd suggest that they are chemically stable and potentially synthesizable experimentally, except for MnSnCu, because its formation energy is positive.

3.2 Elastic properties

A material's elastic constants are fundamental to its mechanical behavior, and understanding them is essential for successful engineering design. A cubic crystal structure has three independent elastic constants, C_{11}, C_{12}, and C_{44}. The condition for mechanical stability of a cubic structure is defined by the Born–Huang criteria [52], [53], [54]:

$$\begin{gathered} C_{11} > 0; \quad C_{44} > 0; \quad C_{11} - C_{12} > 0; \\ C_{11} + 2C_{12} > 0; \quad C_{12} < B < C_{11} \end{gathered} \quad (3)$$

These elastic constants can be used to obtain the values of other important mechanical parameters such as bulk modulus (B), shear modulus (G), Young's modulus (E), Pugh's ratio (B/G), Poisson's ratio (ν), and the anisotropy factor (A), which can be calculated by the following relations [53], [54], [55]:

$$B = \frac{C_{11} + 2C_{12}}{3} \quad (4)$$

$$G_V = \frac{C_{11} - C_{12} - 3C_{44}}{5} \quad (5)$$

$$G_R = \frac{5C_{44}(C_{11} - C_{12})}{4C_{44} + 3(C_{11} - C_{12})} \quad (6)$$

$$G = \frac{G_V + G_R}{2} \quad (7)$$

$$E = \frac{9BG}{3B + G} \quad (8)$$

$$\nu = \frac{3B - E}{6B} \quad (9)$$

$$A = \frac{2C_{44}}{C_{11} - C_{12}} \quad (10)$$

We have also estimated the Cauchy pressure ($C_P = C_{12} - C_{44}$) [56] which provides information

about ductility and brittleness of the material. A negative value of C_P indicates brittleness, whereas a positive value indicates ductile behavior. Table 2 includes the calculated elastic constants and other elastic parameters within the GGA approximation. It is found that all the calculated values of elastic constants lie within the mechanical stability conditions given by Equation (3), which indicates that all the compounds are mechanically stable. Pugh's criterion suggests that materials with a B/G ratio greater than 1.75 are ductile; otherwise, they are brittle [57]. Our results show that the B/G ratios of all the alloys are less than 1.75; therefore, they are brittle in nature. The ductile and brittle behavior can also be interpreted using the Frantsevich rule [58]. If the Poisson's ratio (ν) is less than 0.26, the material is brittle; otherwise, it is ductile. The calculated values of ν reveal that the compounds exhibit brittle behavior (Table 2).

The bonding characteristics of materials can also be predicted by the Poisson's ratio: it is less than 0.1 for covalent materials and greater than or equal to 0.25 for ionic materials [59]. In this regard, the studied materials are found to exhibit covalent bonding. In addition, the negative values of C_P also indicate that all the compounds are brittle in nature. The anisotropy parameter (A) is equal to 1 for isotropic crystals; otherwise, the material is anisotropic. From Table 2, it is seen that all the compounds have anisotropic character. The calculated values, being greater than 1, signify that these alloys exhibit significant elastic anisotropy, which could potentially lead to an increased likelihood of micro-cracks or structural defects during experimental growth.

The Young's modulus (E), defined as the ratio of tensile stress to tensile strain (stiffness), has calculated values of 435.37, 332.28, and 391.46 GPa for MnSnNi, MnSnCu, and MnSnPd, respectively, revealing MnSnNi to be the stiffest among them. The values of the bulk modulus (B) and shear modulus (G) are connected to the longitudinal (v_l), transverse (v_t), and average (v_m) sound velocities of elastic wave propagation, as well as the Debye temperature (θ_D). The following equations can be employed to calculate these quantities [55], [60]:

$$v_l = \left(\frac{3B + 4G}{3\rho}\right)^{1/2} \tag{11}$$

$$v_t = \left(\frac{G}{\rho}\right)^{1/2} \tag{12}$$

$$v_m = \left[\frac{1}{3}\left(\frac{2}{v_t^3} + \frac{1}{v_l^3}\right)\right]^{-1/3} \tag{13}$$

$$\theta_D = \frac{h}{k_B}\left[\frac{3n}{4\pi} \cdot \frac{N_A \rho}{M}\right]^{1/3} v_m \tag{14}$$

Table 2: The calculated values of elastic constants (C_{ij}), bulk modulus (B), shear modulus (G), Young's modulus (E), Poisson's ratio (ν), Pugh's ratio (B/G), anisotropy factor (A), Cauchy's pressure (C_P), longitudinal sound velocity (v_l), transverse sound velocity (v_t), mean sound velocity (v_m), and Debye temperature (θ_D) for MnSnX (X = Ni, Cu, and Pd).

Parameter	**Compound**		
	MnSnNi	MnSnCu	MnSnPd
C_{11} (GPa)	356.42	253.72	300.97
C_{12} (GPa)	-4.41	16.82	3.35
C_{44} (GPa)	309.28	238.80	300.36
B (GPa)	115.86	95.72	102.56
G (GPa)	249.14	180.22	226.58
E (GPa)	435.37	332.28	391.46
ν	-0.126	-0.070	-0.136
B/G	0.46	0.53	-0.13
A	1.71	2.01	2.01
C_P (GPa)	-313.69	-221.97	-297.01
v_l (m s^{-1})	7669.74	6829.03	7183.56
v_t (m s^{-1})	5719.26	5000.79	5375.28
v_m (m s^{-1})	6148.41	5392.42	5775.17
θ_D (K)	713.53	610.14	635.89

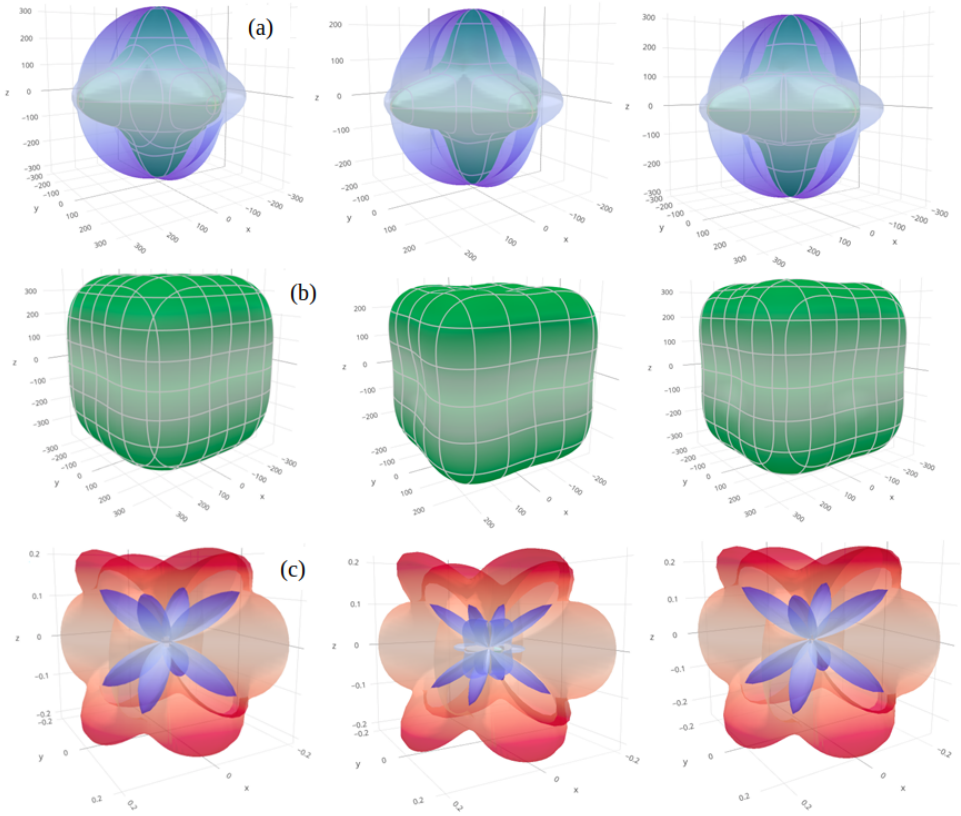

Figure 2: 3D elastic properties of half-Hesler MnSnNi, MnSnCu, and MnSnPd alloys (a) shear modulus (b) Young's modulus, and (c) Poisson's ratio.

Table 3: The minimum and maximum values of shear modulus (G), Young's modulus (E), and Poisson's ratio (ν) of half-Heusler MnSnX (X = Ni, Cu, and Pd) alloys.

Compound	G (GPa)		E (GPa)		ν	
	G_{min}	G_{max}	E_{min}	E_{max}	ν_{min}	ν_{max}
MnSnNi	180.42	309.28	356.31	490.98	-0.27	-0.01
MnSnCu	118.45	238.81	251.63	391.27	-0.28	0.08
MnSnPd	148.81	300.36	300.90	455.97	-0.32	0.01

Further, the 3D elastic characteristics, including shear modulus (G), Young's modulus (E), and Poisson's ratio (ν), were computed for the compounds and visualized using the ELATE program [41], [54], [61] (Figure 2). The 3D profiles of elastic properties suggest a pronounced elastic anisotropy in the materials, particularly evident in the substantial deviation in G and E shapes. Anisotropy predictions were further examined by assessing the minimum and maximum values of these properties, summarized in Table 3 along with ν. The significant disparities between the minimum and maximum values of G and E underscore the high anisotropy within the studied materials. Specifically, MnSnNi, MnSnCu, and MnSnPd exhibit minimum G values of 180.42, 118.45, and 148.81 GPa, respectively, considerably lower than their corresponding maximum values. Likewise, minimum (maximum) E values are 356.31 (490.98) GPa for MnSnNi, 251.63 (391.27) GPa for MnSnCu, and 300.90 (455.97) GPa for MnSnPd. Notably, the minimum G values and maximum E values are consistently found along the same [001] direction, except for MnSnCu. These results suggest that MnSnNi and MnSnPd are more resistant to external pressure along the [001] direction, while simultaneously exhibiting lower shear resistance compared to other crystal orientations. Despite the calculated Poisson's ratio indicating brittleness in Table 2, values extracted from the 3D elastic property profiles range from -0.27 to -0.01, -0.28 to 0.08, and -0.32 to 0.01 for MnSnNi, MnSnCu, and MnSnPd, respectively, indicating overall brittleness in all crystal directions.

3.3 Electronic and magnetic properties

The electronic and magnetic properties of the materials have been studied with the help of spin-projected band structures along the W–L–Γ–X–W–K high-symmetry points and projected density of states (PDOS). The spin-up (↑) (red) and spin-down (↓) (blue) polarized band structures within the GGA approximation are presented in Figure A2 (Appendix). At the Fermi level, it can be seen that there is state overlapping, which destroys the half-metallicity. The presence of *d*-orbitals in the valence shells of Mn, Ni, Cu, and Pd elements provides additional energy levels that contribute to band overlap. This overlap allows electrons to move freely, leading to electrical conductivity. Therefore, there is no band gap between the majority-spin and minority-spin channels of all these compounds, and hence they behave as conductors. Similar results are obtained for all the compounds using the GGA+U method (Figure A3, Appendix) and the mBJ method (Figure 3(a–c)). In order to understand the origin of metallic electronic states near the Fermi level, we also determined the total and partial density of states (DOS) of the materials using the GGA method (see Appendix, Figure A4), GGA+U method (Appendix, Figure A5), and mBJ method (Figure 4(a–c)), respectively. It is clearly shown that the band gap in both spin-up (majority) and spin-down (minority) states is zero, indicating metallic character in all cases.

The electronic configurations of the constituent atoms are Mn = $3d^5 4s^2$, Sn = $4d^{10} 5s^2 5p^2$, Ni = $3d^8 4s^2$, Cu = $3d^{10} 4s^1$, and Pd = $4d^{10}$. These plots reveal that the Mn–3*d* states dominate near the Fermi level and destroy the band gap in both spin channels by crossing the Fermi level.

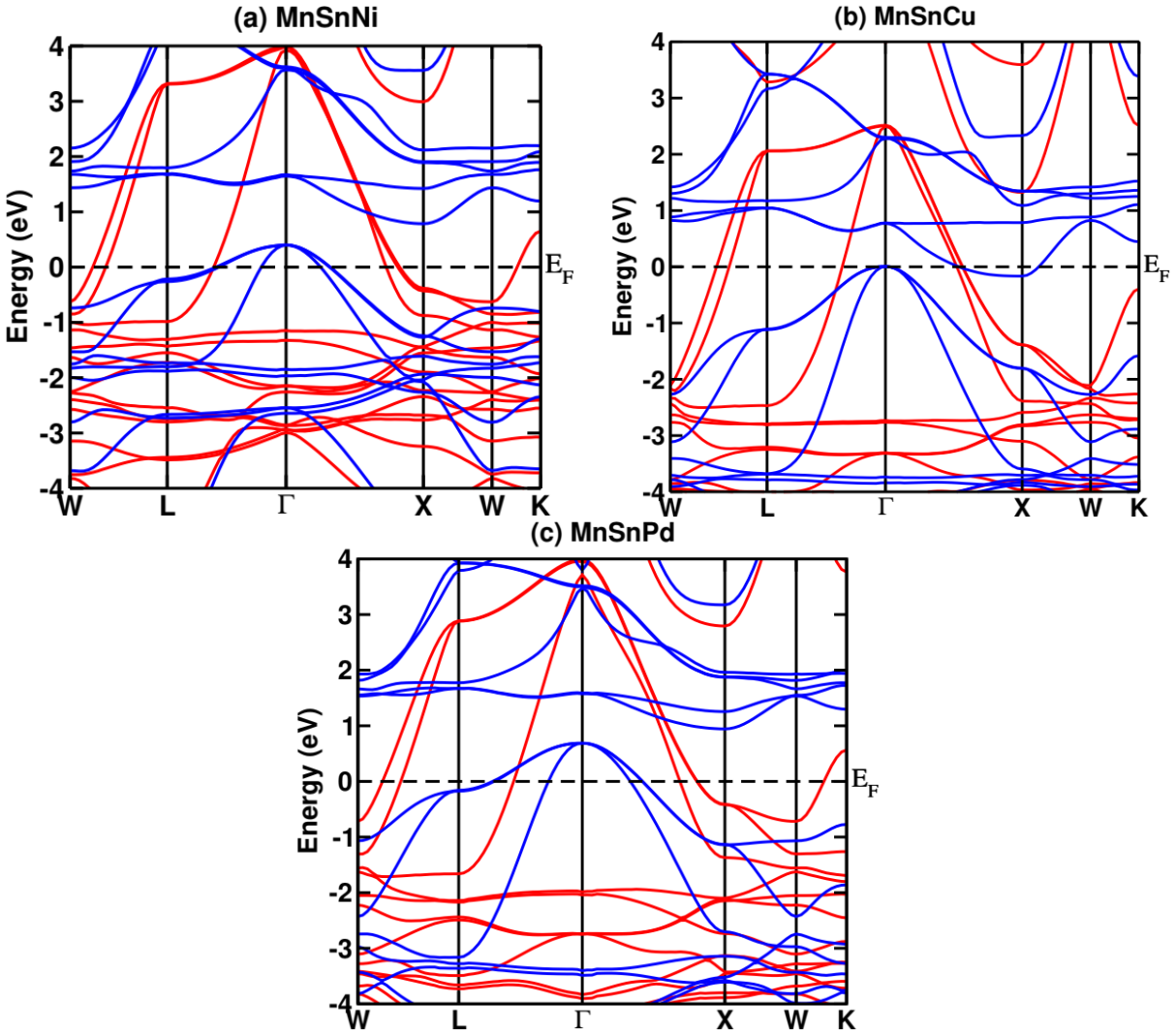

Figure 3: The calculated spin-polarized band structure for spin-up (red) spin-down (blue) channels in unstrained MnSnX (X = Ni, Cu and Pd) with mBJ method.

Due to the absence of a band gap in both spin states, these compounds do not exhibit half-metallic (HM) behavior and instead show metallic character. Further, we have computed total and partial magnetic moments for all compounds under GGA, GGA + U, and mBJ methods (Table 4). It can be observed that the total magnetic moments remains nearly almost same under both GGA and mBJ approximations. This is because spin magnetic moment of Sn atom has negative value which means that its spin is anti-parallel with small magnitude and have a ferromagnetic (FM) ordering with other elements (Ni, Cu and Pd). These opposing magnetic moments tend to cancel each other, leading to an overall magnetic moment that remains unchanged under both approximations. Moreover, the atom Mn has the most contribution to the total magnetic moment with small impact of Ni, Cu, Pd and Sn atoms because of large exchange-splitting of Mn-d state. However, upon the implementation of Hubbard-potential (U), a notable enhancement is observed. This enhancement can be attributed to the intensified electron-electron interactions, resulting in stronger magnetic effects within the system.

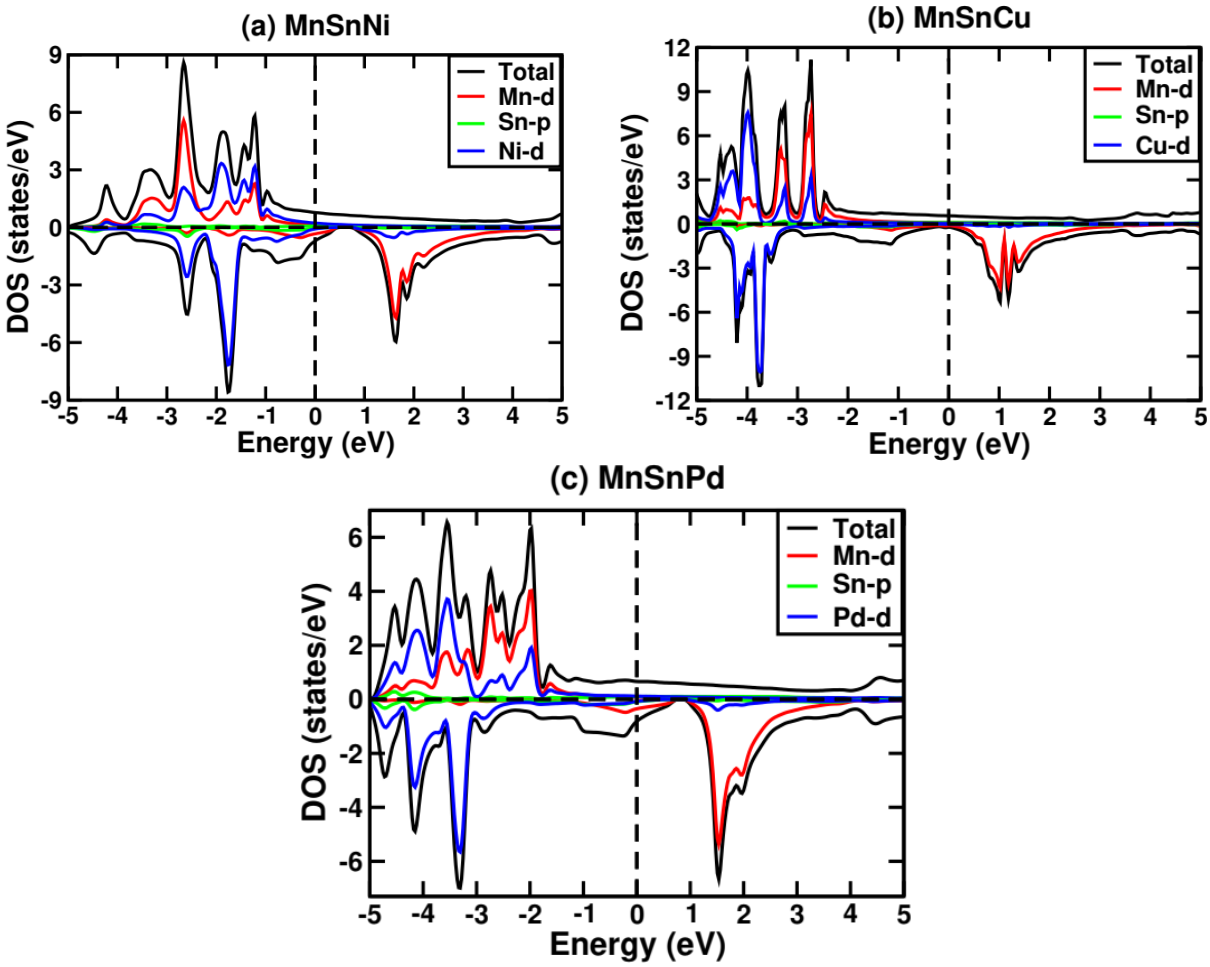

Figure 4: The calculated spin-polarized total and paritial density of states for unstrained MnSnX (X = Ni, Cu and Pd) with mBJ method.

4 Effects of uniform strain

There are numerous potential applications of half-metallicity in spintronic technology, where only one of the two spin orientations of electrons contributes to electrical conduction while the other is completely suppressed. The technique of strain engineering is a prominent and effective approach for fine-tuning the electronic and magnetic properties of materials, primarily through modulation of lattice parameters to achieve desired outcomes [62], [63].

This phenomenon arises due to variations in the contribution of different atomic orbitals with distinct characteristics under the influence of strain. Compressive strain shifts the Fermi level toward higher energy, while tensile strain shifts it toward lower energy. Subsequently, we examined how uni-

Table 4: The local magnetic moments of Mn (M_{Mn}), Sn (M_{Sn}), and X (M_X; X = Ni, Cu, Pd), interstitial magnetic moment (M_I), and total magnetic moment (M_T) of half-Heusler MnSnX (X = Ni, Cu, and Pd) alloys.

Compound	Method	M_{Mn}	M_{Sn}	M_X	M_I	M_T
MnSnNi	GGA	3.424	-0.118	0.062	0.062	3.312
	GGA+U	3.989	-0.112	0.022	-0.025	3.873
	mBJ	3.659	-0.160	0.086	-0.248	3.337
MnSnCu	GGA	3.886	-0.066	0.054	0.099	3.974
	GGA+U	4.201	-0.097	0.005	0.052	4.162
	mBJ	4.027	-0.080	0.035	-0.017	3.963
MnSnPd	GGA	3.871	-0.129	0.035	-0.051	3.725
	GGA+U	4.276	-0.109	4.276	-0.010	4.189
	mBJ	4.011	-0.181	0.038	-0.266	3.601

form compressive and tensile strains influence the electronic and magnetic properties of the materials. The optimized lattice parameter is used as a reference (0% strain), and both compressive and tensile strains are applied within the GGA and mBJ frameworks. The influence of strain on the electronic states was assessed by analyzing the total density of states (TDOS) under different strain conditions, as illustrated in Figure A6 (Appendix) using the GGA method and Figure 5 using the mBJ method. In the case of tensile strain, the TDOS exhibits nearly identical features to the unstrained (0%) case in both methods.

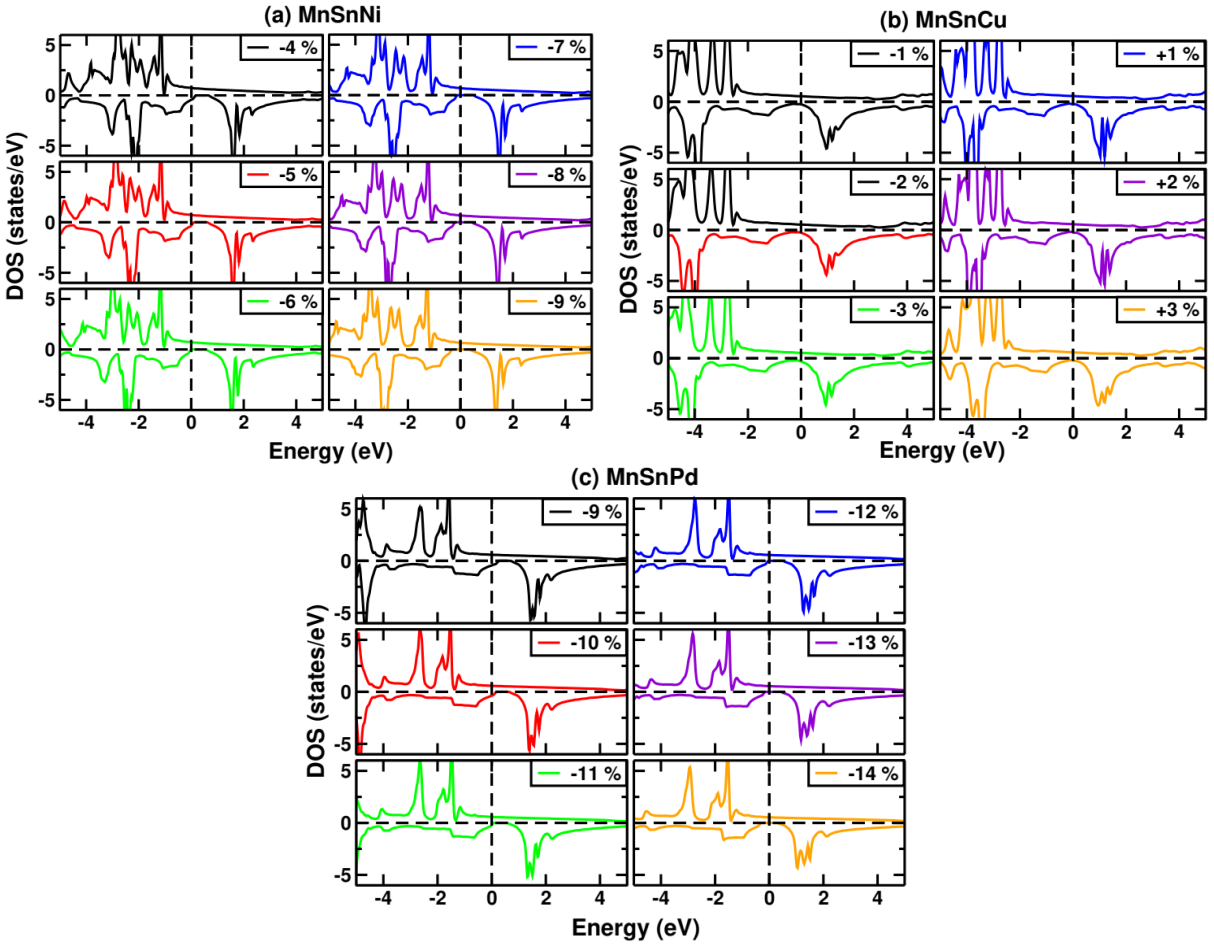

Figure 5: The calculated spin-polarized total density of states (TDOS) under uniform strains with mBJ method of half-Heusler MnSnX (X=Ni, Cu and Pd) alloys.

Furthermore, systems under compressive strain from -1% to -4% for MnSnNi and -1% to -8% for MnSnPd also show TDOS profiles nearly identical to the unstrained system within the GGA method. Interestingly, with increasing compressive strain, the Fermi level in the minority-spin channel shifts significantly toward higher energies. These shifts occur at strain from -5% to -9% for MnSnNi and -9% to -14% for MnSnPd, causing the minority-spin states to no longer intersect the Fermi energy (E_F). However, the majority-spin channel continues to cross E_F, indicating metallic behavior. Overall, this confirms the emergence of half-metallic electronic states with 100% spin polarization, in contrast to the behavior of the unstrained system.

In order to visually depict the variations in electronic characteristics under uniform strain, we also plotted the computed band gap (E_g) as a function of strain using both the GGA method (Figure A7, Appendix) and the mBJ method (Figure 6). The calculated values of the band gap for MnSnNi are 0.656, 0.697, 0.739, 0.780, and 0.822 eV at -5%, -6%, -7%, -8%, and -9%, respectively. For MnSnPd, the corresponding values are 0.693, 0.733, 0.776, 0.797, 0.799, and 0.800 eV at -9%, -10%, -11%, -12%, -13%, and -14%, respectively. This indicates that -5% and -9% compressive strain are sufficient to tune the electronic properties of MnSnNi and MnSnPd within the GGA method. Furthermore, similar half-metallic behavior is observed (except for MnSnCu) from -6% to -9% for MnSnNi and -12% to -14% for MnSnPd using the mBJ method. Beyond these limits, all compounds exhibit metallic character. The calculated band gaps for MnSnNi are 0.609, 0.655, 0.675, and 0.716 eV at -6%, -7%, -8%, and -9%, respectively. For MnSnPd, the band gaps are 0.575, 0.618, and 0.654 eV at -12%, -13%, and -14%, respectively. A small increment in the band gap is observed using the GGA method from -5% to -9% and -9% to -14%, while it becomes zero beyond these limits for MnSnNi and MnSnPd, respectively. The decrease in the band gap is linked to enhanced hybridization between Mn–3d and Ni–34d, Cu–3d, and Pd–4d states, as compressive strain strengthens atomic interactions and increases orbital overlap, resulting in broader bandwidth and reduced energy gap, as explained in Refs. [63], [64].

Furthermore, using the mBJ method, the band gap increases from -6% to -9% for MnSnNi, and -12% to -14% for MnSnPd. Beyond these limits no band gap appears. However, the band gap remains nearly zero for MnSnCu within the mBJ method. Thus, no half-metallic behavior is observed for MnSnCu due to the states crossing both majority and minority spin channels. Next, we investigated the strain-induced variations of the total and local magnetic moments as a function of strain for all compounds using the GGA method (Figure A8, Appendix) and the mBJ method (Figure 7). The results show that the total magnetic moment remains constant at 3.00 μ_B from -5% to -9% for MnSnNi and -9% to -14% for MnSnPd within the GGA method. Similarly, no change in the total magnetic moment is observed using the mBJ method for MnSnNi from -6% to -9% and MnSnPd from -12% to -14%, except for MnSnCu. Thus, the integer value of the total magnetic moment confirms the robustness of half-metallicity for MnSnNi and MnSnPd, following the Slater–Pauling rule $M_t = Z_t - 18$, with 100% spin polarization at the Fermi level within the GGA method. With the mBJ method, only MnSnNi and MnSnPd follow the Slater–Pauling rule. The spin magnetic moment of Mn increases after applying the mBJ correction compared to GGA, while the total magnetic moment remains unchanged in the region of half-metallic character. This behavior arises because Mn contributes the largest positive spin magnetic moment, whereas Ni, Cu, Pd, and Sn atoms are aligned antiparallel, leading to mutual cancellation and a nearly constant total magnetic moment under both approximations. The obtained results indicate that the magnetic moment in each compound is primarily contributed by the Mn atoms, with very small contributions from Ni, Cu, Pd, and Sn atoms.

5 Conclusion

We studied the structural, elastic, and strain effects on the electronic and magnetic properties of half-Heusler MnSnX (X = Cu, Ni, and Pd) alloys using spin-polarized density functional theory (DFT) calculations. The calculated negative formation and cohesive energies indicate that these compounds are chemically stable and potentially synthesizable, except for MnSnCu. In addition, elastic property analysis reveals that all compounds are mechanically stable and exhibit brittle nature. The electronic structure analysis shows half-metallic (HM) behavior under uniform compressive strain from -5% to -9% for MnSnNi and -9% to -14% for MnSnPd within the GGA method, which is in contrast to the unstrained case. Similarly, HM behavior is confirmed using the mBJ method, except for MnSnCu, at strain from -6% to -9% for MnSnNi and -12% to -14% for MnSnPd. In these cases, one spin

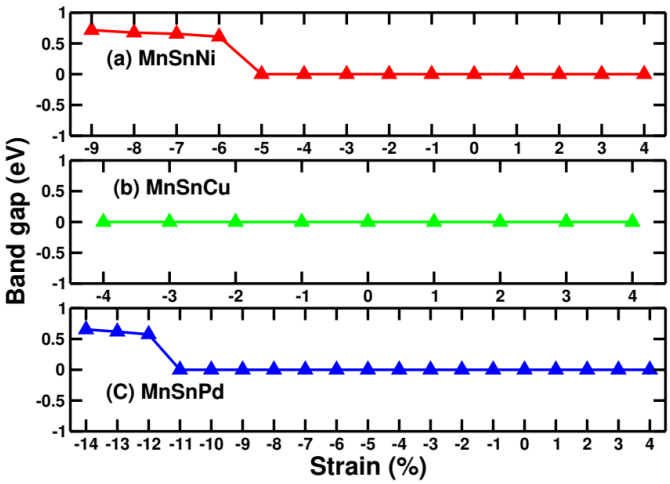

Figure 6: Calculated band gaps under different strains for half-Heusler MnSnX (X=Ni, Cu and Pd) alloys with mBJ method.

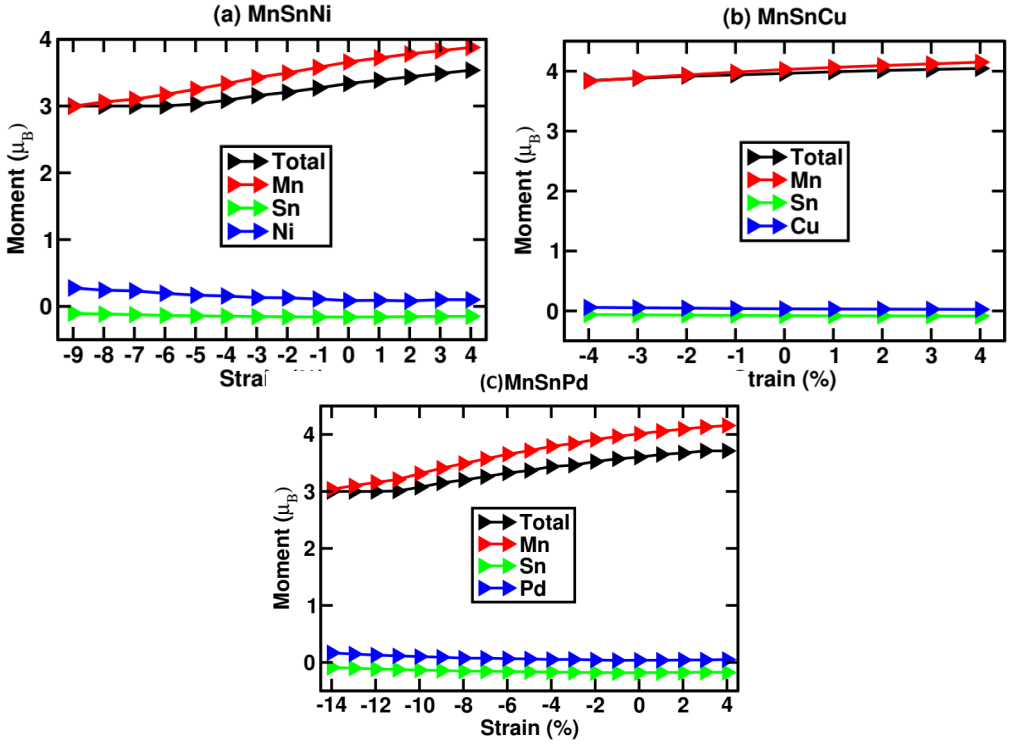

Figure 7: Calculated total and local magnetic moments of MnSnX (X = Ni, Cu and Pd) under uniform strain with mBJ method.

channel is metallic while the other exhibits an insulating character with a finite band gap. Beyond these strain limits, the systems undergo significant structural changes, making them unsuitable for reliable electronic or spintronic applications.

The magnetic properties under compressive strain, where HM behavior is observed, satisfy the Slater–Pauling 18-electron rule with 100% spin polarization near the Fermi level. This magnetic behavior is mainly contributed by Mn atoms, with minor contributions from Ni, Pd, and Sn atoms. However, MnSnCu does not exhibit HM behavior under either ambient or strained conditions. Overall, these results suggest that the electronic and magnetic properties of MnSnNi and MnSnPd can be effectively tuned via strain engineering for potential spintronic applications.

References

[1] De Groot RA, Mueller FM, van Engen PG, Buschow KHJ. New class of materials: half-metallic ferromagnets. Physical Review Letters. 1983;50(25):2024.

[2] Zhao JS, Gao Q, Li L, Xie HH, Hu XR, Xu CL, et al. First-principles study of the structure, electronic, magnetic and elastic properties of half-Heusler compounds LiXGe (X= Ca, Sr and Ba). Intermetallics. 2017;89:65-73.

[3] Birsan A, Palade P, Kuncser V. Half-metallic state and magnetic properties versus the lattice constant in Ti2CoSn Heusler compound: An ab initio study. Solid State Communications. 2012;152(24):2147-50.

[4] Ahmad R, Mehmood N. A first principle study of half-Heusler compounds CrTiZ (Z= P, As). Journal of Superconductivity and Novel Magnetism. 2018;31(1):257-64.

[5] Arshad H, Zafar M, Ahmad S, Rizwan M, Khan MI, Gillani SSA, et al. Theoretical study of structural, electronic and magnetic properties of equiatomic quaternary CoPdCrZ (Z= Si, Ge, P) Heusler alloys. Modern Physics Letters B. 2019;33(31):1950389.

[6] Gilleßen M, Dronskowski R. A combinatorial study of full Heusler alloys by first-principles computational methods. Journal of Computational Chemistry. 2009;30(8):1290-9.

[7] Gofryk K, Kaczorowski D, Plackowski T, Mucha J, Leithe-Jasper A, Schnelle W, et al. Magnetic, transport, and thermal properties of the half-Heusler compounds ErPdSb and YPdSb. Physical Review B—Condensed Matter and Materials Physics. 2007;75(22):224426.

[8] Galanakis I, Mavropoulos P, Dederichs PH. Electronic structure and Slater–Pauling behaviour in half-metallic Heusler alloys calculated from first principles. Journal of Physics D: Applied Physics. 2006;39(5):765-75.

[9] Babiker S, Gao G, Yao K. Half-metallicity and magnetism of Heusler alloys Co2HfZ (Z= Al, Ga, Ge, Sn). Journal of Magnetism and Magnetic Materials. 2017;441:356-60.

[10] De Teresa JM, Serrate D, Ritter C, Blasco J, Ibarra MR, Morellon L, et al. Investigation of the high Curie temperature in Sr 2 Cr Re O 6. Physical Review B—Condensed Matter and Materials Physics. 2005;71(9):092408.

[11] Fecher GH, Ebke D, Ouardi S, Agrestini S, Kuo CY, Hollmann N, et al. State of Co and Mn in half-metallic ferromagnet Co2MnSi explored by magnetic circular dichroism in hard X-ray photoelectron emission and soft X-ray absorption spectroscopies. In: Spin. vol. 4. World Scientific; 2014. p. 1440017.

[12] Zhang YJ, Wang WH, Zhang HG, Liu EK, Ma RS, Wu GH. Structure and magnetic properties of Fe2NiZ (Z= Al, Ga, Si and Ge) Heusler alloys. Physica B: Condensed Matter. 2013;420:86-9.

[13] Nehra J, Lakshmi N, Venugopalan K. Effect of substitution of Co with Fe on the structural, electronic and magnetic properties of Heusler alloy Co2CrAl. Physica B: Condensed Matter. 2015;459:46-51.

[14] Djaafri T, Djaafri A, Saadaoui F. First-principles investigation of ferromagnetic, thermodynamic, elastic, and half-metallic behavior of ReCrTe and RuCrTe half-Heusler alloys. Journal of Superconductivity and Novel Magnetism. 2018;31(8):2449-58.

[15] Chibani S, Arbouche O, Zemouli M, Benallou Y, Amara K, Chami N, et al. First-principles investigation of structural, mechanical, electronic, and thermoelectric properties of Half-Heusler compounds RuVX (X= As, P, and Sb). Computational Condensed Matter. 2018;16:e00312.

[16] Rahman N, Husain M, Yang J, Murtaza G, Sajjad M, Habib A, et al. First principle study of structural, electronic, elastic, and magnetic properties of half-Heusler compounds ScTiX (X= Si, Ge, Pb, In, Sb, and Tl). Journal of Superconductivity and Novel Magnetism. 2020;33(12):3915-22.

[17] Shakil M, Hassan S, Arshad H, Rizwan M, Gillani SSA, Rafique M, et al. Theoretical investigation of structural, magnetic and elastic properties of half Heusler LiCrZ (Z= P, As, Bi, Sb) alloys. Physica B: Condensed Matter. 2019;575:411677.

[18] Bennani MA, Aziz Z, Terkhi S, Elandaloussi EH, Bouadjemi B, Chenine D, et al. Structural, electronic, magnetic, elastic, thermodynamic, and thermoelectric properties of the half-Heusler RhFeX (with X= Ge, Sn) compounds. Journal of Superconductivity and Novel Magnetism. 2021;34(1):211-25.

[19] Shakil M, Kousar M, Gillani SSA, Rizwan M, Arshad H, Rafique M, et al. First principle computation of half metallicity and mechanical properties of a new series of half Heusler alloys KMnZ (Z= B, Si, Ge, As) for spintronics. Indian Journal of Physics. 2022;96(1):115-26.

[20] Radouan D, Anissa B, Benaouda B. Investigation of electronic, optical, and thermoelectric properties of new d0 half-metallic half-heusler alloys SiLiX (C= Ca and Sr). Emergent Materials. 2022;5(4):1097-108.

[21] Sattar MA, Rashid M, Rasool MN, Mahmood A, Hashmi MR, Ahmad SA, et al. Half-metallic ferromagnetism in new half-Heusler compounds: an ab initio study of CrTiX (X= Si, Ge, Sn, Pb). Journal of Superconductivity and Novel Magnetism. 2016;29(4):931-8.

[22] Mehmood N, Ahmad R. Structural, electronic, magnetic, and optical properties of half-Heusler alloys RuMnZ (Z= P, As): a first-principle study. Journal of Superconductivity and Novel Magnetism. 2018;31(1):233-9.

[23] Javed M, Sattar MA, Benkraouda M, Amrane N. Structural and mechanical stability, lattice dynamics and electronic structure of the novel CrVZ (Z= S, Se, & Te) half-Heusler alloys. Materials Today Communications. 2020;25:101519.

[24] Khandy SA, Islam I, Kaur K, Ali AM, Abd El-Rehim AF. Effect of strain on the electronic structure and phonon stability of SrBaSn half heusler alloy. Molecules. 2022;27(12):3785.

[25] Wanasinghe D, Aslani F. A review on recent advancement of electromagnetic interference shielding novel metallic materials and processes. Composites Part B: Engineering. 2019;176:107207.

[26] He JY, Wang H, Huang HL, Xu XD, Chen MW, Wu Y, et al. A precipitation-hardened high-entropy alloy with outstanding tensile properties. Acta Materialia. 2016;102:187-96.

[27] Valiev RZ, Murashkin MY, Sabirov I. A nanostructural design to produce high-strength Al alloys with enhanced electrical conductivity. Scripta Materialia. 2014;76:13-6.

[28] Hohenberg P, Kohn W. Inhomogeneous electron gas. Physical Review. 1964;136(3B):B864.

[29] Casper F, Graf T, Chadov S, Balke B, Felser C. Half-Heusler compounds: novel materials for energy and spintronic applications. Semiconductor Science and Technology. 2012;27(6):063001.

[30] Perdew JP, Chevary JA, Vosko SH, Jackson KA, Pederson MR, Singh DJ, et al. Atoms, molecules, solids, and surfaces: Applications of the generalized gradient approximation for exchange and correlation. Physical Review B. 1992;46(11):6671.

[31] Farshchi R, Ramsteiner M. Spin injection from Heusler alloys into semiconductors: A materials perspective. Journal of Applied Physics. 2013;113(19).

[32] Kammerer S, Thomas A, Hutten A, Reiss G. Co2MnSi Heusler alloy as magnetic electrodes in magnetic tunnel junctions. Applied Physics Letters. 2004;85(1):79-81.

[33] Tanaka CT, Nowak J, Moodera JS. Spin-polarized tunneling in a half-metallic ferromagnet. Journal of Applied Physics. 1999;86(11):6239-42.

[34] Xiong ZH, Wu D, Valy Vardeny Z, Shi J. Giant magnetoresistance in organic spin-valves. Nature. 2004;427(6977):821-4.

[35] Hordequin C, Nozieres JP, Pierre J. Half metallic NiMnSb-based spin-valve structures. Journal of Magnetism and Magnetic Materials. 1998;183(1-2):225-31.

[36] Wang P, Xia JB, Wu HB. Electronic structures, magnetic properties and strain effects of quaternary Heusler alloys FeMnCrZ (Z= P, As, Sb, Bi, Se, Te). Journal of Magnetism and Magnetic Materials. 2019;490:165490.

[37] Bai J, Ji J, Hao L, Yang T, Tan X. DFT investigation on the electronic, magnetic, mechanical properties and strain effects of the quaternary compound Cu2FeSnS4. Crystals. 2020;10(6):509.

[38] Ray RB, Kaphle GC, Rai RK, Yadav DK, Paudel R, Paudyal D. Strain induced electronic structure, and magnetic and structural

properties in quaternary Heusler alloys ZrRhTiZ (Z= Al, In). Journal of Alloys and Compounds. 2021;867:158906.

[39] Blaha P, Schwarz K, Sorantin P, Trickey SB. Full-potential, linearized augmented plane wave programs for crystalline systems. Computer Physics Communications. 1990;59(2):399-415.

[40] Schwarz K, Blaha P. Solid state calculations using WIEN2k. Computational Materials Science. 2003;28(2):259-73.

[41] Yadav S, Chaudhary U, Kaphle G. Exploring the structural, elastic, electronic, and optical properties of Na-based hydrides X3NaH4 (X= K, Rb) for hydrogen storage applications: A First-principles study. International Journal of Hydrogen Energy. 2025;160:150637.

[42] Chaudhary U, Kaphle G, Yadav S. Pressure-dependent structural, elastic, electronic, thermodynamic, and optical properties of LuGaO3 perovskite: A first-principles study. AIP Advances. 2025;15(8).

[43] Chaudhary U, Chaudhary S, Yadav DK, Kaphle GC, Yadav SK. First-Principles Investigation of Structural, Elastic, Electronic, and Optical Properties of AcMO3 (M= B, Sc) Perovskites. physica status solidi (b). 2025;262(5):2400574.

[44] Perdew JP, Burke K, Ernzerhof M. Generalized gradient approximation made simple. Physical Review Letters. 1996;77(18):3865.

[45] Anisimov VI, Zaanen J, Andersen OK. Band theory and Mott insulators: Hubbard U instead of Stoner I. Physical Review B. 1991;44(3):943.

[46] Liechtenstein AI, Anisimov VI, Zaanen J. Density-functional theory and strong interactions: Orbital ordering in Mott-Hubbard insulators. Physical Review B. 1995;52(8):R5467.

[47] Tran F, Blaha P. Accurate Band Gaps of Semiconductors and Insulators with a Semilocal Exchange-Correlation Potential. Physical Review Letters. 2009;102(22):226401.

[48] Hamri B, Abbar B, Hamri A, Baraka O, Hallouche A, Zaoui A. Electronic structure and mechanical properties of X2MnSn (X=Cu, Ni, Pd) under hydrostatic pressure: GGA+U calculations. Computational Condensed Matter. 2015;3:14-20.

[49] Murnaghan FD. The compressibility of media under extreme pressures. Proceedings of the National Academy of Sciences. 1944;30(9):244-7.

[50] Saal JE, Kirklin S, Aykol M, Meredig B, Wolverton C. Materials design and discovery with high-throughput density functional theory: the open quantum materials database (OQMD). JOM. 2013;65(11):1501-9.

[51] Kirklin S, Saal JE, Meredig B, Thompson A, Doak JW, Aykol M, et al. The Open Quantum Materials Database (OQMD): assessing the accuracy of DFT formation energies. npj Computational Materials. 2015;1(1):1-15.

[52] Born M, Huang K. Dynamical theory and experiment I. Publishers, Berlin. 1982.

[53] Yadav S, Dahal S, Khadka R, Guragain B, Pokharel P, Oli P, et al. First-principles study of electronic, vibrational, elastic and thermodynamic properties of Sc-X (X= C, N, O) compounds. Pramana. 2026;100(2):53.

[54] Dahal S, Sapkota DR, Khadka D, Guragain B, Chaudhary U, Yadav S. Ab initio analysis of structural and physical properties of MgX (X= Ag, Au) alloys. BIBECHANA. 2026;23(1):93-104.

[55] Osafile OE, Azi JO. First principles prediction of structural, mechanical and thermodynamic stability in new 18-valence electron XVZ (X= Fe, Ni, Z= Ga, As) half-Heusler semiconductors. Semiconductor Science and Technology. 2020;35(10):105005.

[56] Pettifor DG. Theoretical predictions of structure and related properties of intermetallics. Materials Science and Technology. 1992;8(4):345-9.

[57] Pugh SF. XCII. Relations between the elastic moduli and the plastic properties of polycrystalline pure metals. The London, Edinburgh, and Dublin Philosophical Magazine and Journal of Science. 1954;45(367):823-43.

[58] Frantsevich IN. Elastic constants and elastic moduli of metals and insulators. Reference Book. 1982.

[59] Haines J, Leger JM, Bocquillon G. Synthesis and design of superhard materials. Annual Review of Materials Research. 2001;31(1):1-23.

[60] Wachter P, Filzmoser M, Rebizant J. Electronic and elastic properties of the light actinide tellurides. Physica B: Condensed Matter. 2001;293(3-4):199-223.

[61] Gaillac R, Pullumbi P, Coudert FX. ELATE: an open-source online application for analysis and visualization of elastic tensors. Journal of Physics: Condensed Matter. 2016;28(27):275201.

[62] Qian Y, Wu H, Kan E, Lu J, Lu R, Liu Y, et al. Biaxial strain effect on the electronic and magnetic phase transitions in double perovskite La2FeMnO6: A first-principles study. Journal of Applied Physics. 2013;114(6).

[63] Lu R, Wu H, Qian Y, Kan E, Liu Y, Tan W, et al. The effect of biaxial mechanical strain on the physical properties of double perovskite Sr2FeMoO6: A theoretical study. Solid State Communications. 2014;191:70-5.

[64] Hung YC, Jiang JC, Chao CY, Su WF, Lin ST. Theoretical Study on the Correlation between Band Gap, Bandwidth, and Oscillator Strength in Fluorene-Based Donor- Acceptor Conjugated Copolymers. The Journal of Physical Chemistry B. 2009;113(24):8268-77.

Appendix

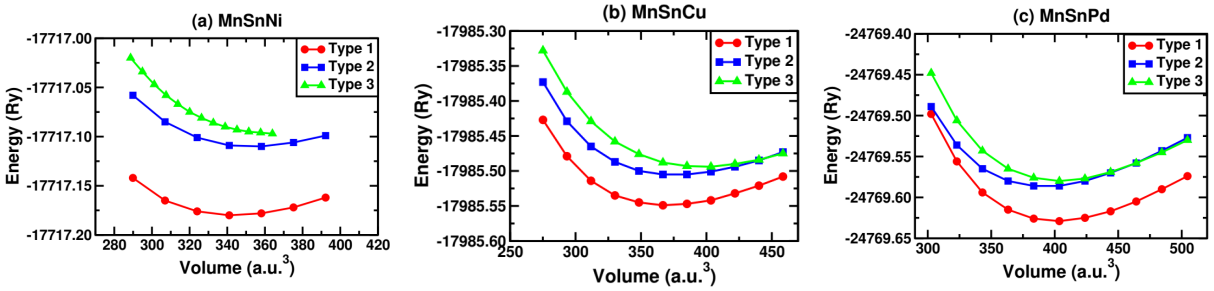

Figure 1A: Volume optimization at various atomic positions (Type 1, Type 2, Type 3) for MnSnX (X = Ni, Cu, and Pd).

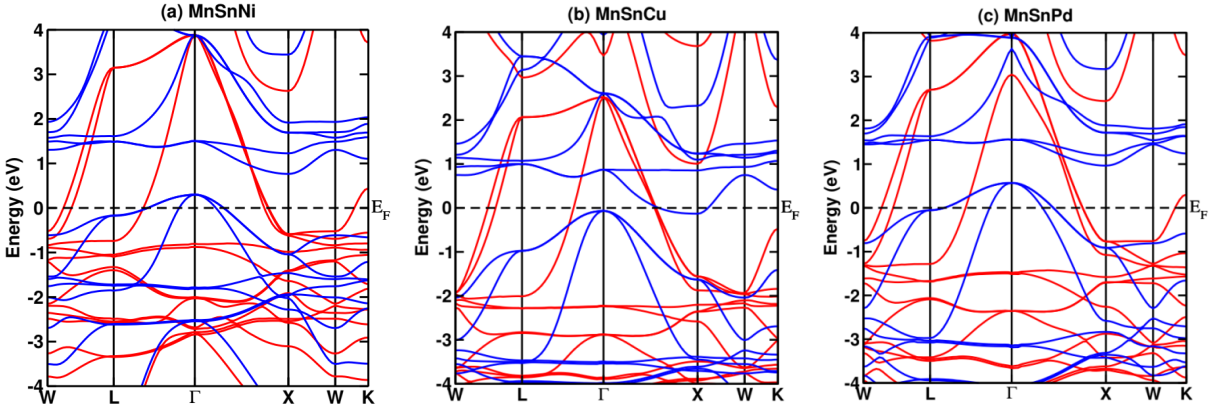

Figure 2A: The calculated spin-polarized band structure for spin-up (red) spin-down (blue) channels in unstrained MnSnX (X = Ni, Cu, and Pd) with GGA method.

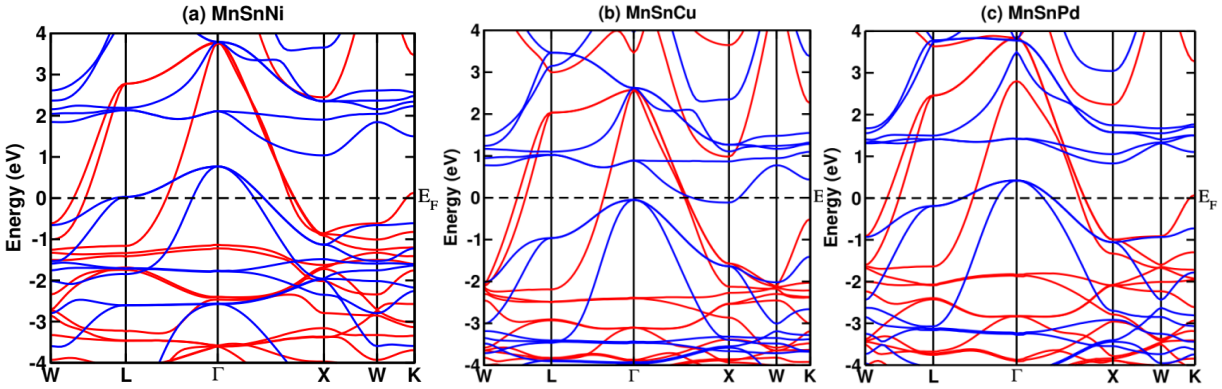

Figure 3A: The calculated spin-polarized band structure for spin-up (red) and spin-down (blue) channels in unstrained MnSnX (X = Ni, Cu, and Pd) with GGA+U method.

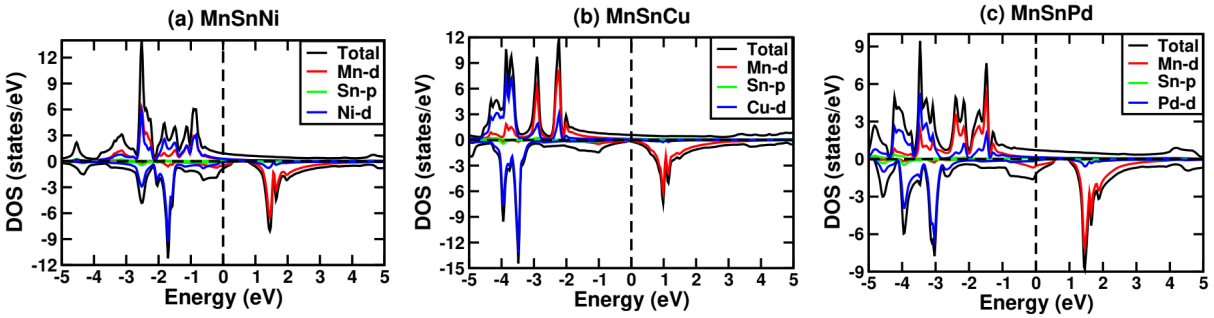

Figure 4A: The calculated spin-polarized total and partial density of states for unstrained MnSnX (X = Ni, Cu and Pd) with GGA method.

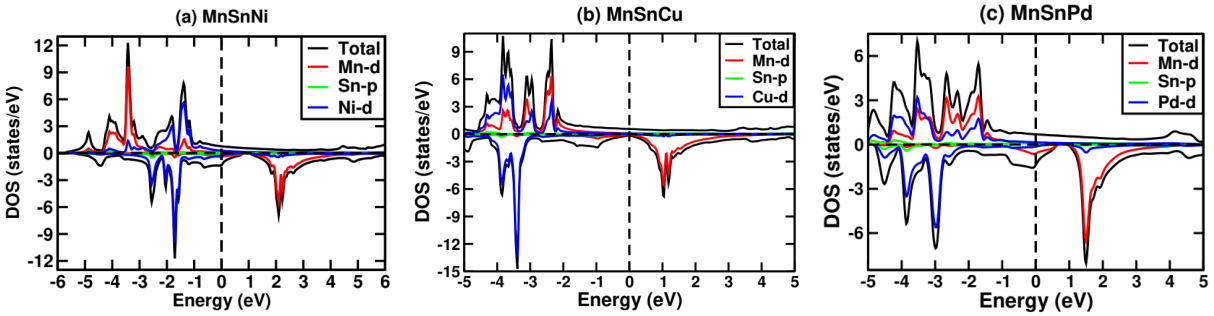

Figure 5A: The calculated spin-polarized total and partial density of states for unstrained MnSnX (X = Ni, Cu, and Pd) with GGA+U method.

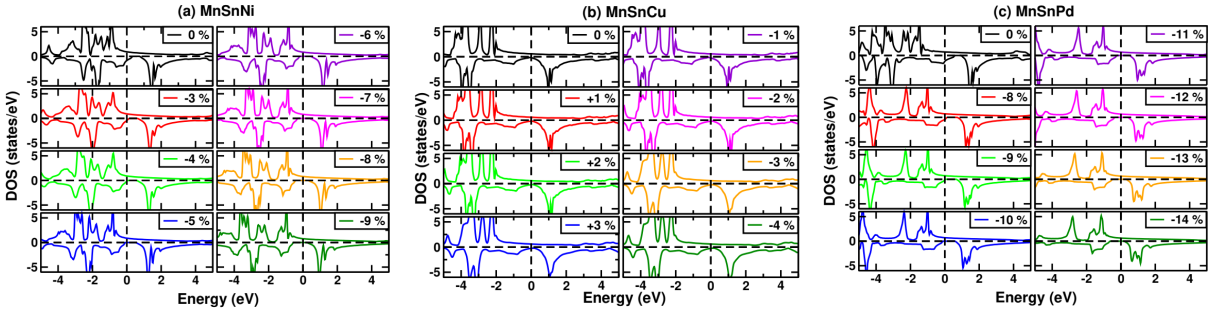

Figure 6A: The calculated spin-polarized total density of states (TDOS) under uniform strains with GGA method.

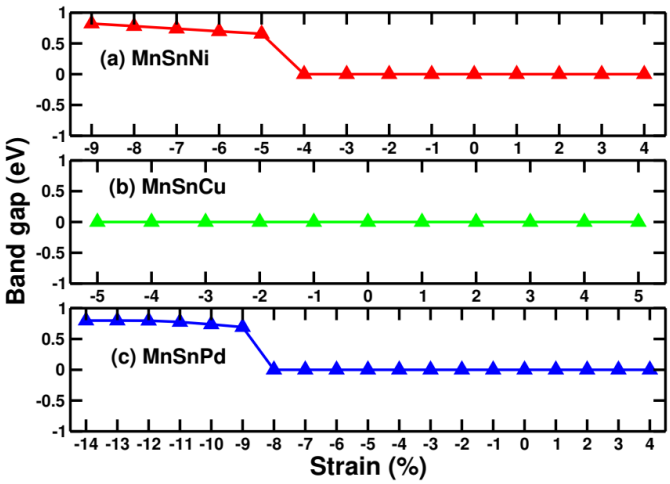

Figure 7A: Calculated band gaps under different strains for half-Heusler MnSnX (X=Ni, Cu and Pd) alloys with GGA method.

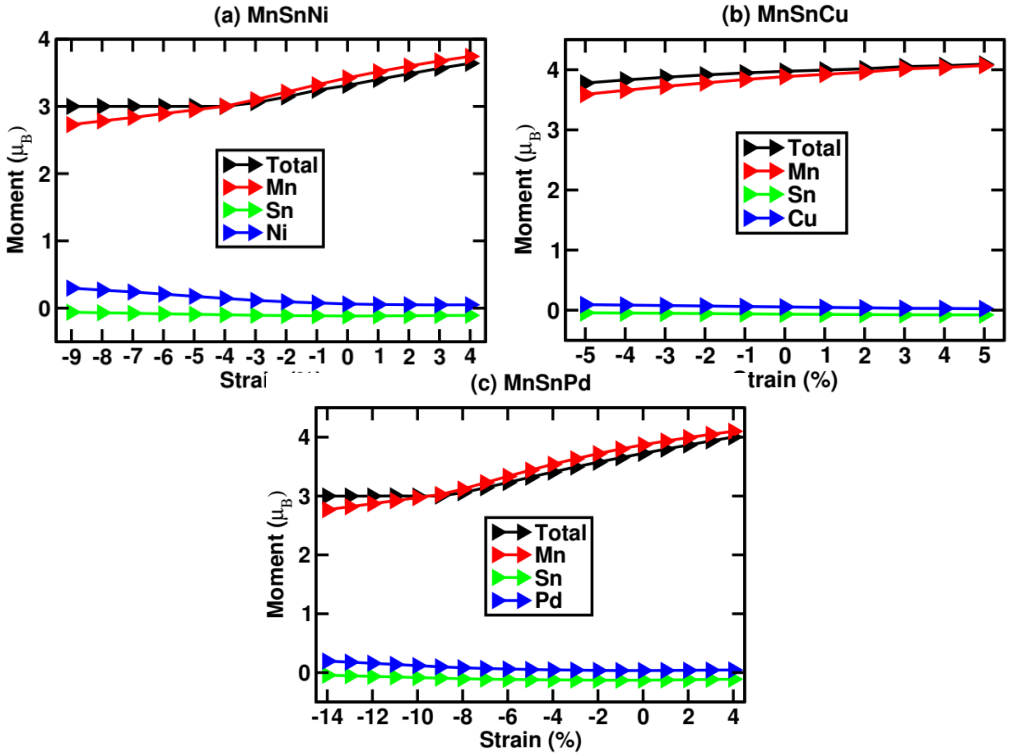

Figure 8A: Calculated total and local magnetic moments of MnSnX (X = Ni, Cu and Pd) under uniform strain with GGA method.